NATIONAL ADVISORY COMMITTEE FOR AERONAUTICS

TECHNICAL NOTE 4182

PHYSICAL CHARACTERISTICS

AND TEST CONDITIONS OF AN ETHYLENE-HEATED
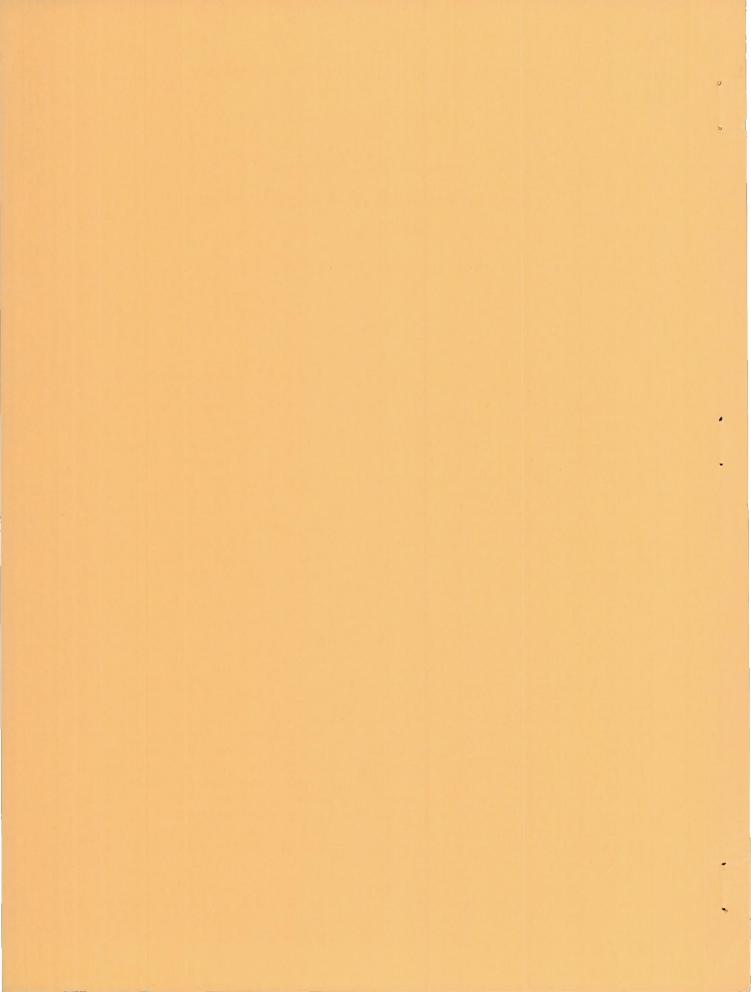
HIGH-TEMPERATURE JET

By Roland D. English, Abraham Spinak,
and Eldred H. Helton

Langley Aeronautical Laboratory
Langley Field, Va.

NACA

Washington
January 1958

L

PHYSICAL CHARACTERISTICS

AND TEST CONDITIONS OF AN ETHYLENE-HEATED

HIGH-TEMPERATURE JET

By Roland D. English, Abraham Spinak,
and Eldred H. Helton

SUMMARY

In order to investigate the effects of high temperatures incurred at hypersonic speeds, an ethylene-heated high-temperature jet has been developed at the Langley Pilotless Aircraft Research Station at Wallops Island, Va. The jet utilizes the combustion of ethylene $\left(C_2H_4\right)$ to produce a supersonic stream in which tests may be made at stagnation temperatures up to nearly 5,000° R. The stagnation temperature and static and stagnation pressure profiles have been measured at centerline stagnation temperatures up to about 3,600° R. The thermal properties of the exhaust gas and flow conditions in the test section have been calculated. The results show the test section Mach number to be about 2.03. Reynolds numbers based on a length of 1 foot varied from about 14×10^6 at a stagnation temperature of 1,000° R to about 2×10^6 at a stagnation temperature of nearly 5,000° R. Corresponding Prandtl numbers varied between 0.721 and 0.622.

INTRODUCTION

In order to study the effects on missile components of the high temperatures incurred at hypersonic speeds, a ground test facility was developed at the Langley Pilotless Aircraft Research Station at Wallops Island, Va., which is capable of producing stagnation temperatures near 5,000° R. Although the facility has been in operation for some time, it was only after recent modifications that fairly uniform test conditions were obtained. This paper was prepared to provide prospective users of the facility with a reference containing a description of these test conditions, the dimensions of the test region, and the calculated thermal properties of the exhaust gas. These data will also be of use to personnel concerned with the development of similar facilities in the future.

SYMBOLS

c_p specific heat at constant pressure, Btu/lb-°F

k thermal conductivity, Btu/ft-sec-°F

M Mach number

N_{Pr} Prandtl number, $c_p\mu/k$

N_{Re} Reynolds number

p_f fuel injection pressure, lb/sq in.

p_∞ free-stream static pressure, lb/sq in.

$p_{t,\infty}$ free-stream stagnation pressure at nozzle exit, lb/sq in.

$p_{t,1}$ free-stream stagnation pressure upstream of burner, lb/sq in.

$p_{t,2}$ stagnation pressure behind a normal shock, lb/sq in.

R ideal gas constant, $53.3 \dfrac{\text{ft-lb}}{\text{lb-}°\text{R}}$

r nozzle radius, in.

T_∞ exit static temperature, °R

$T_{t,\infty}$ exit stagnation temperature, °R

x longitudinal coordinates of nozzle, in.

γ ratio of specific heats

μ absolute viscosity, lb/ft-sec

ρ_∞ free-stream density at nozzle exit, slugs/cu ft

DESCRIPTION

The ethylene-heated high-temperature jet at the Langley Pilotless Aircraft Research Station at Wallops Island, Va., is a blowdown jet system consisting of a 12-inch-diameter steel duct leading away from storage spheres to a convergent-divergent stainless-steel nozzle. Air is kept in the storage spheres at a pressure of about 200 pounds per square inch and a dewpoint of about -40° F. During operation, air from the spheres is preheated to approximately 900° R and passed through the duct into a combustion chamber where ethylene is injected into the air-stream from a doughnut-type Inconel burner. The ethylene is ignited by firing a small solid-propellant rocket into the ethylene-air mixture. The products of the resulting combustion are passed through the nozzle and exhausted at ambient sea-level pressure to obtain shock-free flow. The temperature of the exhaust gas is varied by changing the ratio of the mass flow of fuel to the mass flow of air (fuel-air ratio). The static pressure is maintained at the sea-level value by regulating the stagnation pressure upstream of the burner. Fuel flow is controlled by a dome control valve in the fuel line outside the tunnel and air flow is controlled by a rotary valve located at the air exit from the storage spheres.

A hydraulically operated, pivoted model support is provided for swinging models into the test section after equilibrium conditions are reached. This support is capable of swinging a model from its position outside the jet to the center line of the test section in 0.2 second. At the completion of the test, the model is swung out of the jet before tunnel shutdown. Thus, the model is not subjected to the relatively high aerodynamic forces and temperatures which occur during the starting and shutdown of the jet.

A sketch of the tunnel and model support is shown as figure 1. A photograph of the tunnel with a model in the test section is shown as figure 2(a). Figure 2(b) is a photograph of the tunnel exit and survey rake which was used in the calibration of the tunnel at high temperatures.

The burner currently used to inject the fuel into the combustion chamber consists of three concentric hollow Inconel tubes supported by straight Inconel tubes on a hollow steel sting. The outside diameter of the largest ring is 10 inches. During operation the fuel is passed through the sting and supports into the rings where it is sprayed into the airstream from rows of orifices on the inner and outer elements of each ring. It should be noted that the present burner is a development of other types of burners used earlier. The first burner tested con-sisted of several layers of rings which were 8 inches in outside diam-eter. Experience showed that large gradients occurred in the tempera-ture profiles obtained with this burner. Consequently, the diameter of

the outer rings was increased to 10 inches and the inner rings were
enlarged proportionately. This second burner was the one used in the
tunnel calibration, a description of which follows. During the cali-
bration tests, it was found that the second burner failed structurally
after relatively few runs. In order to alleviate the drag loads and
thermal stresses set up by unequal heating rates, layers of rings were
systematically removed until the minimum number necessary to support
combustion was found. These tests showed that a single layer of rings
was sufficient and resulted in the burner used currently and described
previously. A photograph of the burner currently in use is shown in
figure 3(a). A drawing of the burner used during tunnel calibration
is shown in figure 3(b).

TUNNEL CALIBRATION

In order to determine the flow conditions in the tunnel test sec-
tion, a survey rake (see sketch in fig. 4) was constructed. The rake
contained a row of shielded bare wire thermocouples (platinum and plat-
inum plus 13-percent rhodium) in one plane and a row of pitot-static
probes in the perpendicular plane. A series of calibration runs was
made during which stagnation temperature and static and stagnation
pressures were recorded continuously. During the calibration runs, the
tips of the pressure probes were located from 1/2 inch to 1 inch from
the tunnel exit. Typical measured stagnation temperature profiles are
shown in figure 5. Included in the figure for comparison are some
stagnation temperature profiles measured by thermocouples in the 12-inch
duct $3\frac{1}{2}$ inches upstream of the nozzle throat. Typical static- and

stagnation-pressure profiles are shown in figure 6. It should be noted
that the values of stagnation pressure presented are those occurring
downstream of a normal shock since there were bow waves standing in
front of the pressure probes. The blunt-nosed probes were required to
withstand the high temperatures incurred.

Since it is impossible to have a survey rake in the test section
during tests on a model, it was necessary to develop some other means
of measuring stagnation temperature during test runs. Several methods
of determining stagnation temperature were investigated during the cali-
bration tests, two of which gave satisfactory results. The first was
the use of thermocouples mounted upstream of the test section. (See
fig. 5.) In order to evaluate this method, center-line stagnation tem-
perature measured just upstream of the nozzle throat was plotted against
exit center-line stagnation temperature in figure 7. The temperature
was, in general, slightly higher upstream of the nozzle than at the
exit. The temperatures at the two locations, however, were within
100° F of each other up to $2,600^{\circ}$ R. Temperature upstream of the nozzle

was not measured at higher stagnation temperatures because of the structural failure of the stainless-steel thermocouple supports.

The second method of determining exit stagnation temperature was to determine the temperature variation with some parameter associated with fuel-air ratio. The average stagnation pressure upstream of the burner was taken to be an indication of the mass flow of air and the fuel-injection pressure, an indication of the mass flow of fuel. Exit center-line stagnation temperature is given as a function of the ratio of these two pressures $(p_f/p_{t,1})$ in figure 8. The test points are within about 150° of the faired line through the points at temperatures up to $3,600^\circ$ R, the maximum temperature at which the tunnel was calibrated.

THERMAL PROPERTIES OF THE EXHAUST GAS

The composition by weight of the exhaust gas was calculated, dissociation effects being neglected, by the method presented in reference 1 for fuel-air ratios up to the stoichiometric value of 0.067. This method consists of balancing the chemical equation for the combustion process and assuming that the ethylene is completely converted to carbon dioxide and water vapor. In the calculation, the weight composition of air was assumed to be 23 percent oxygen and 77 percent nitrogen; the elements which are present in small quantities were neglected. The calculated composition of the exhaust gas is shown in figure 9 as a function of fuel-air ratio.

The adiabatic flame temperature of the exhaust gas was calculated by the method of reference 2. As in the calculation of the composition of the exhaust gas, it was assumed that the ethylene was completely oxidized and dissociation effects were neglected. The variation of adiabatic flame temperature with fuel-air ratio is shown in figure 10. The temperatures in figure 10 are based on an air entrance temperature of 900° R. Since the composition of the exhaust gas and the adiabatic flame temperature were known, it was possible to obtain the variation of the specific heat at constant pressure c_p, the ratio of specific heats γ, and the ideal gas constant R of the exhaust gas by the method of reference 1. The variation of the thermal conductivity k and viscosity μ with temperature was obtained by averaging the thermal conductivities and viscosities of the components of the exhaust gas according to their weight composition. The variation with temperature of the thermodynamic properties of the components of the exhaust was obtained from reference 3. Reference 1 shows that the composite ideal gas constant is very close to that of air. The variation with temperature of the specific heat at constant pressure, the ratio of specific

heats, thermal conductivity, and viscosity of the exhaust gas are shown in figure 11.

TEST-SECTION FLOW CONDITIONS

It is desirable, of course, to have as small a stagnation-temperature gradient as possible in the test section. The temperature profiles obtained during the calibration of the preflight high-temperature jet (see fig. 5 for typical profiles) show that, within a 3-inch radius of the center line, the variation in stagnation temperature is within 100° F up to about $2,600^\circ$ R and within 150° F up to about $3,600^\circ$ R. Since a 6-inch diameter is about the maximum for a model of any length because of the limitations of the tunnel exit Mach cone, the region outside the 3-inch radius mentioned previously is of little interest and the "test section" as used hereinafter refers to the region within a 3-inch radius of the center line.

The variation in stagnation pressure (behind a normal shock) is within about 3.5 pounds per square inch in the test section. It should be noted here that, since the completion of the calibration tests reported herein, the flameholder has been modified by the removal of several rings. Since no modification was made to the fuel distribution system, no change in the stagnation temperature profiles is expected. The removal of rings from the flameholder, however, undoubtedly reduced the drop in total pressure across the flameholder and the gradient in the stagnation pressure profiles at the exit should be reduced.

The variation with temperature of the ratio of static pressure to stagnation pressure behind a normal shock was calculated from the Rayleigh pitot equation (ref. 4) by using the calculated values of γ (fig. 11). Then by using the measured static and stagnation pressures and the corresponding measured stagnation temperatures, it was possible to determine the test-section Mach number over the range of temperatures for which the tunnel was calibrated. There was some random variation in Mach number across the test section because of the transient variations in γ from the calculated values. By using the average ratio of static pressure to stagnation pressure for a given temperature, the average test-section Mach number was determined. The results show negligible variation in Mach number with stagnation temperature and the average Mach number was found to be 2.03. The variation of test-section static temperatures with test-section stagnation temperatures was calculated by using the one-dimensional energy equation (ref. 4) and is shown in figure 12.

The test-section static pressure is held as nearly constant as possible at the ambient sea-level value during a test. Since the Mach number remains essentially constant whereas γ varies with temperature, the ratio of static pressure to stagnation pressure varies. The variation with stagnation temperature of the ratio of free-stream static pressure to free-stream stagnation pressure has been calculated from the isentropic channel flow equation (ref. 4) by using the calibrated Mach number (2.03) and the calculated values of γ. The results, together with the free-stream stagnation pressure corresponding to a static pressure of 14.7 pounds per square inch, are shown in figure 13.

The ideal gas law was used to obtain the test-section density based on a static pressure of 14.7 pounds per square inch absolute. The free-stream velocity was calculated by using the thermal properties of the exhaust gas and the calibrated Mach number. The test-section Reynolds number based on a length of 1 foot and the Prandtl number were computed over the range of stagnation temperatures of the tunnel. Density, Reynolds number, and Prandtl number are shown as functions of stagnation temperature in figure 14.

CONCLUDING REMARKS

A series of calibration runs have been made in the ethylene-heated high-temperature jet at the Langley Pilotless Aircraft Research Station at Wallops Island, Va. The results of these calibration runs along with the calculated thermal properties of the exhaust gas were used to determine the test conditions. The test-section Mach number was found to be about 2.03. The Reynolds numbers based on a length of 1 foot varied from approximately 14×10^6 at a stagnation temperature of $1,000^\circ$ R to approximately 2×10^6 at a stagnation temperature of nearly $5,000^\circ$ R. Corresponding Prandtl numbers varied between 0.721 and 0.622.

Langley Aeronautical Laboratory,
     National Advisory Committee for Aeronautics,
          Langley Field, Va., September 20, 1957.

8

REFERENCES

1. Pinkel, Benjamin, and Turner, L. Richard: Thermodynamic Data for the Computation of the Performance of Exhaust-Gas Turbines. NACA WR E-23, 1944. (Formerly NACA ARR 4B25.)

2. Fricke, Edwin F.: Statistical Thermodynamics Applied to Chemical Kinetics of Combustion. Report No. EDR-22-407, Republic Aviation Corp., Oct. 1, 1947.

3. Hilsenrath, Joseph, Beckett, Charles W., et al.: Tables of Thermal Properties of Gases. NBS Cir. 564, U. S. Dept. Commerce, 1955.

4. Ames Research Staff: Equations, Tables, and Charts for Compressible Flow. NACA Rep. 1135, 1953. (Supersedes NACA TN 1428.)

x	r	x	r
0	6.00	11.0	5.44
1.0	5.27	12.0	5.53
2.0	4.77	13.0	5.61
3.0	4.55	14.0	5.69
3.4	4.53	15.0	5.76
4.0	4.55	16.0	5.82
5.0	4.68	17.0	5.86
6.0	4.84	18.0	5.91
7.0	4.97	19.0	5.93
8.0	5.12	20.0	5.96
9.0	5.22	21.0	5.98
10.0	5.35	22.0	6.00
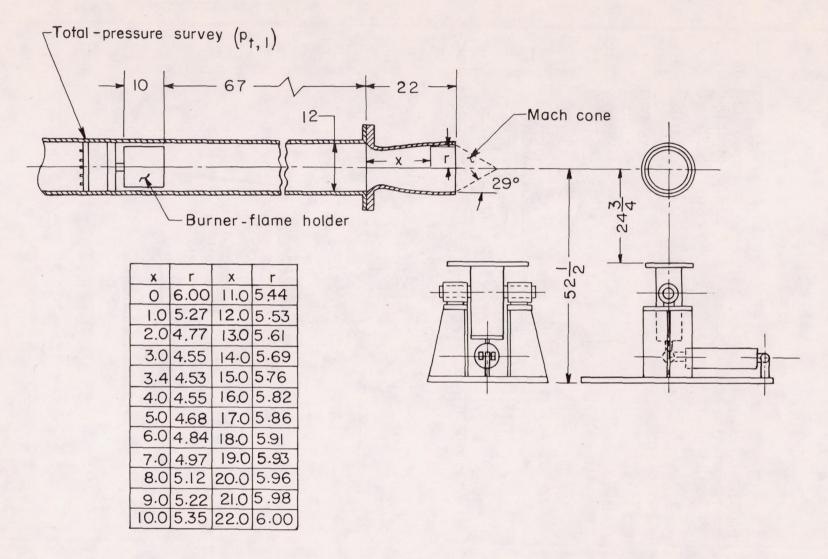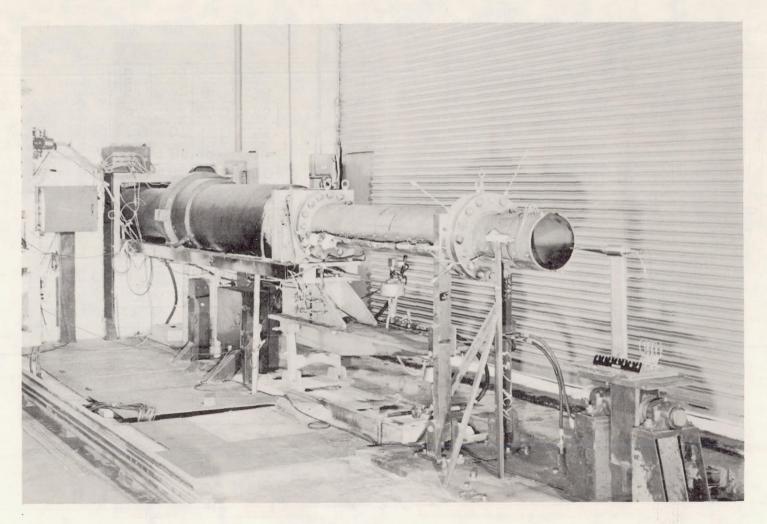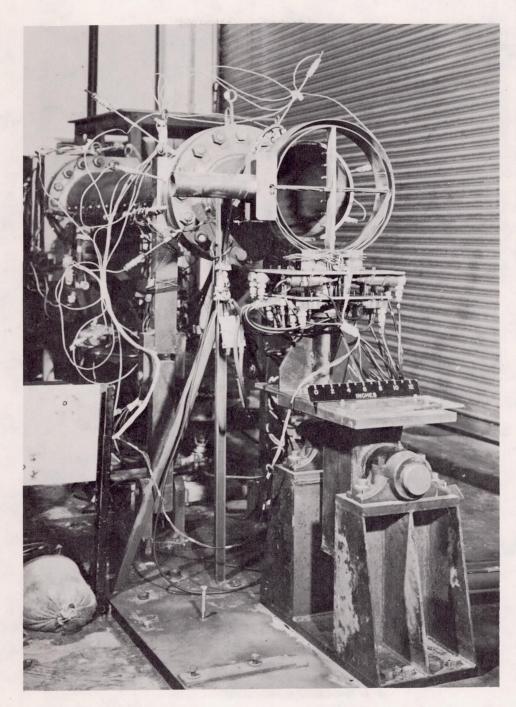
Figure 1.- Sketch of tunnel and model support. All linear dimensions are in inches.

(a) Tunnel with model in test section.   L-95344

Figure 2.- Photographs of tunnel.
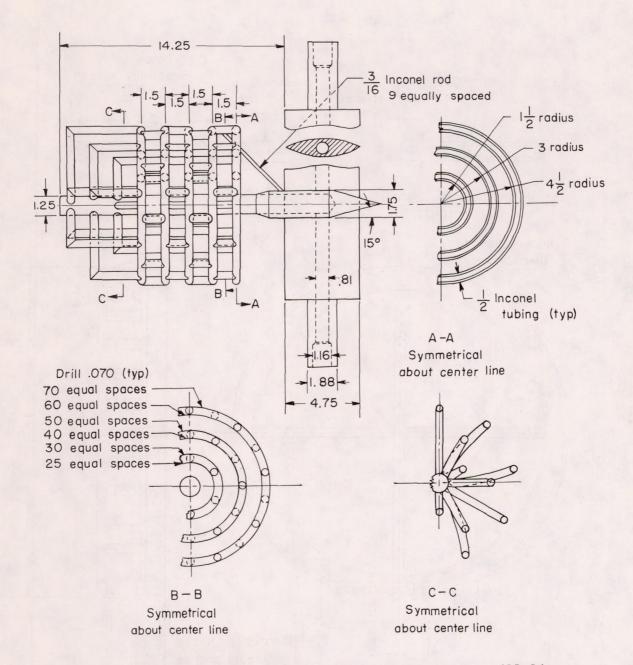
(b) Tunnel exit with survey rake in test section.   L-95233

Figure 2.- Concluded.

(a) Photograph of the burner currently in use.   L-57-2210

Figure 3.- Physical characteristics of the burner.

14.25

1.5 1.5 1.5 1.5

C B A

$\frac{3}{16}$ Inconel rod
9 equally spaced

1.25

C B A

$1\frac{1}{2}$ radius

3 radius

$4\frac{1}{2}$ radius

1.75

15°

$\frac{1}{2}$ Inconel tubing (typ)

.81

A–A
Symmetrical
about center line

1.16

1.88

4.75

Drill .070 (typ)
70 equal spaces
60 equal spaces
50 equal spaces
40 equal spaces
30 equal spaces
25 equal spaces

B–B
Symmetrical
about center line

C–C
Symmetrical
about center line

(b) Sketch of the burner used during tunnel calibration. All linear
dimensions are in inches.

Figure 3.- Concluded.

.033 holes
4 equally spaced

.020 holes
8 equally spaced

$2\frac{1}{2}$

$\frac{3}{8}$

$\frac{1}{4}$

Thermocouple detail
(enlarged)

Pressure probe
detail (enlarged)

8 equally spaced
thermocouples

15

8 equally spaced
pressure probes

$\frac{1}{8}$

$3\frac{1}{2}$

$\frac{1}{2}$

$1\frac{3}{4}$

$3\frac{3}{4}$

17
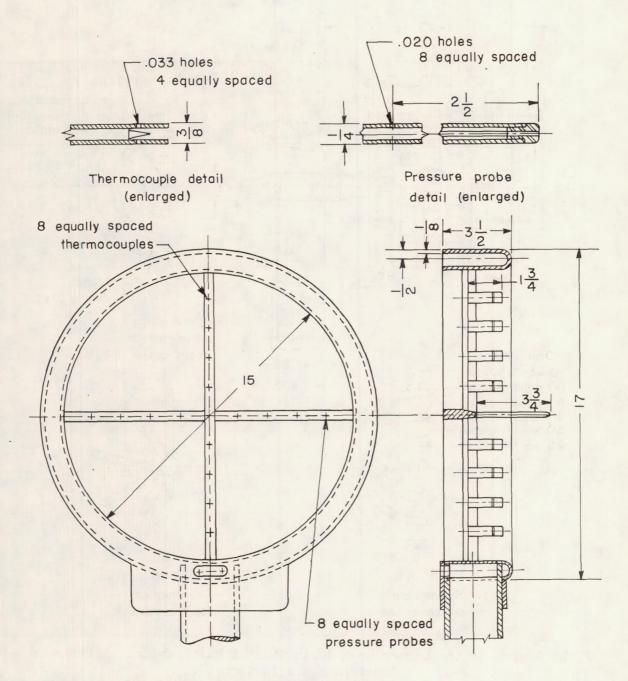
Figure 4.- Sketch of survey rake. All dimensions are in inches.
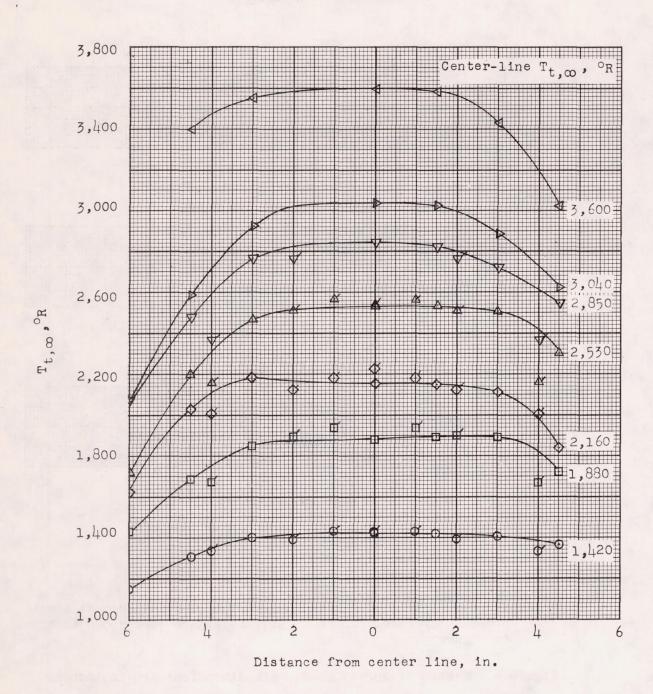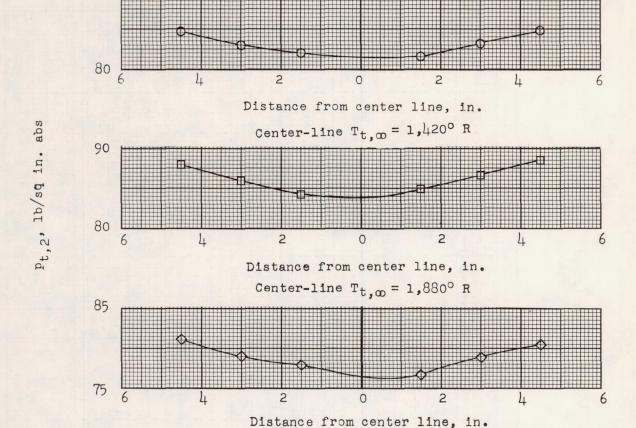
Figure 5.- Typical stagnation temperature profiles. Flagged symbols indicate temperature measured upstream of the nozzle.

(a) Stagnation pressure (behind a normal shock).
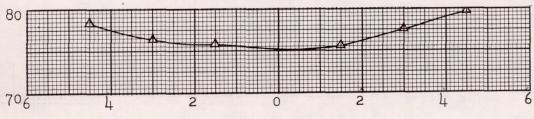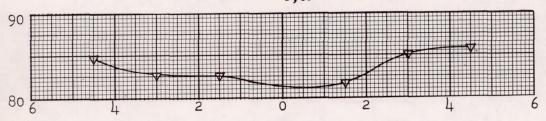
Figure 6.- Typical static and stagnation (behind a normal shock) pressure profiles. Symbols in this figure correspond to those in figure 5.

$p_{t,2}$, lb/sq in. abs

Distance from center line, in.
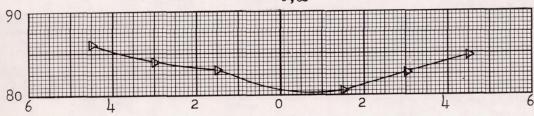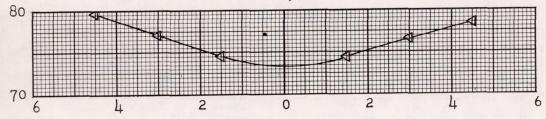
Center-line $T_{t,\infty}$ = 2,530° R

Distance from center line, in.

Center-line $T_{t,\infty}$ = 2,850° R

Distance from center line, in.

Center-line $T_{t,\infty}$ = 3,040° R

Distance from center line, in.
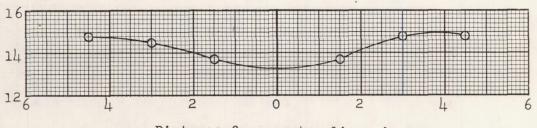
Center-line $T_{t,\infty}$ = 3,600° R

(a) Concluded.

Figure 6.- Continued.
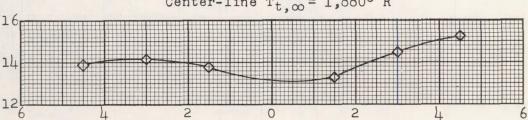
Distance from center line, in.

Center-line $T_{t,\infty} = 1,420^\circ$ R
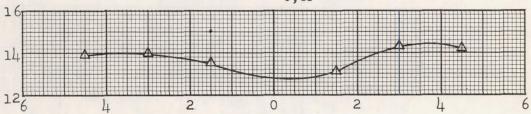
Distance from center line, in.

Center-line $T_{t,\infty} = 1,880^\circ$ R

Distance from center line, in.
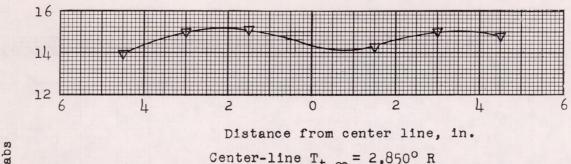
Center-line $T_{t,\infty} = 2,160^\circ$ R

Distance from center line, in.
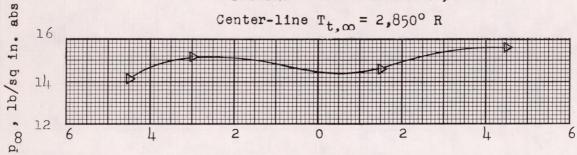
Center-line $T_{t,\infty} = 2,530^\circ$ R
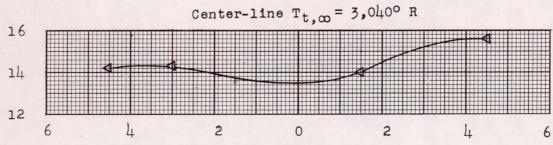
(b) Static pressure.

Figure 6.- Continued.

Distance from center line, in.

Center-line $T_{t,\infty}$ = 2,850° R

Distance from center line, in.

Center-line $T_{t,\infty}$ = 3,040° R

Distance from center line, in.

Center-line $T_{t,\infty}$ = 3,600° R

(b) Concluded.

Figure 6.- Concluded.
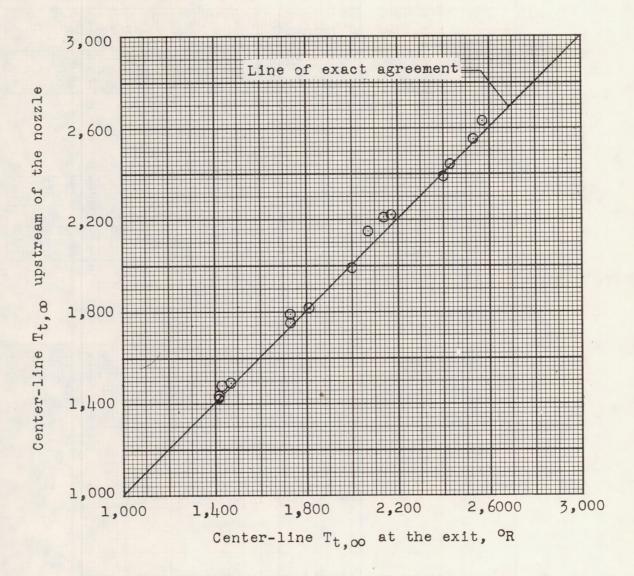
Figure 7.- Comparison of center-line stagnation temperature upstream of the nozzle and at the exit.
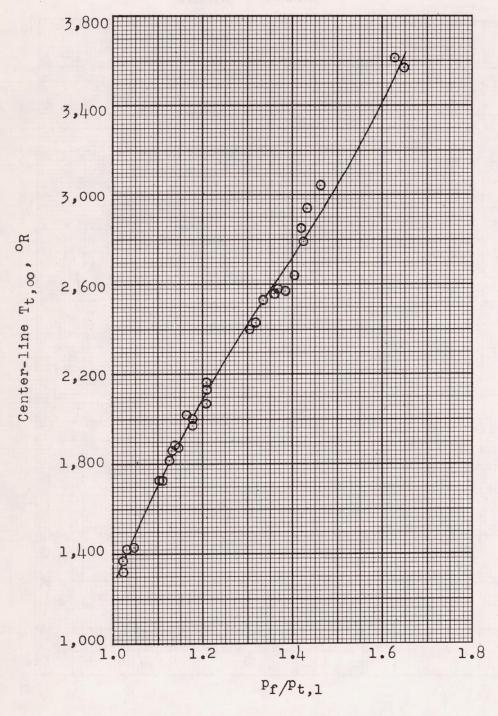
Figure 8.- Variation of center-line stagnation temperature with the ratio of fuel injection pressure to stagnation pressure upstream of the burner.
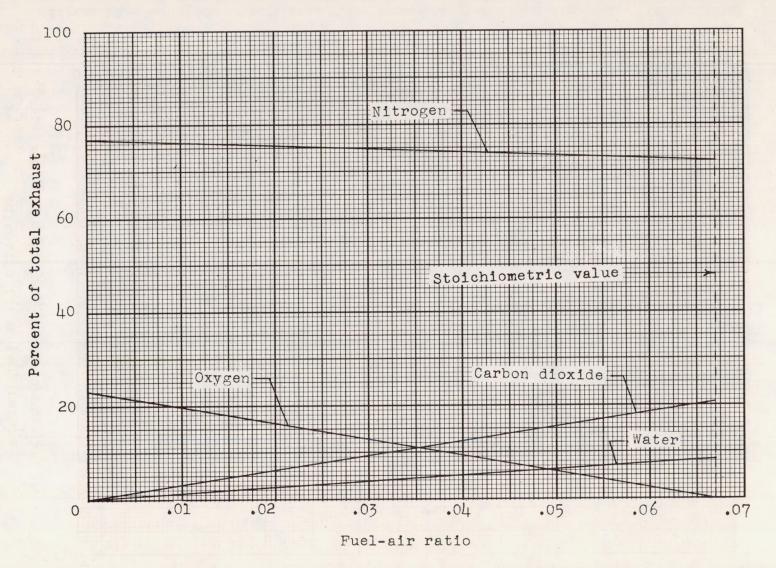
Figure 9.- Variation of the composition of the exhaust gas (neglecting dissociation) with fuel-air ratio.
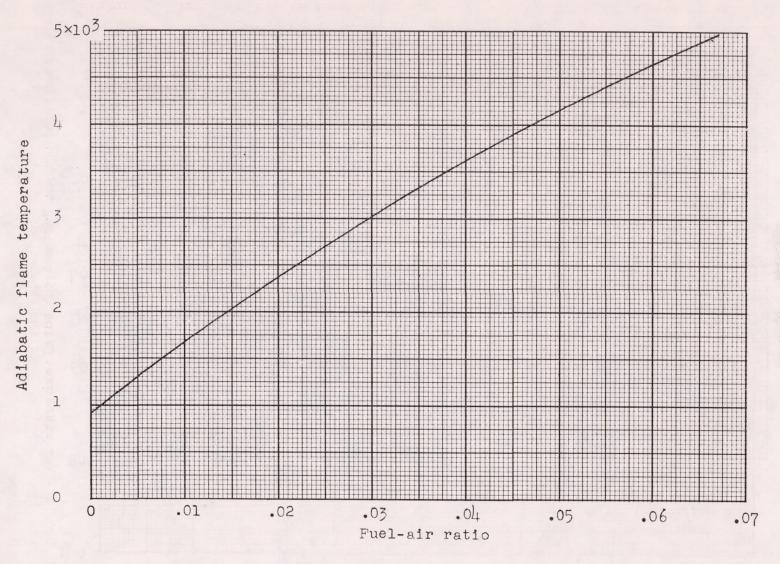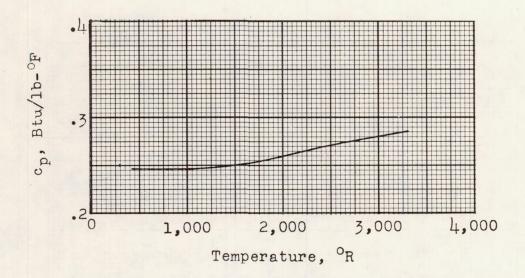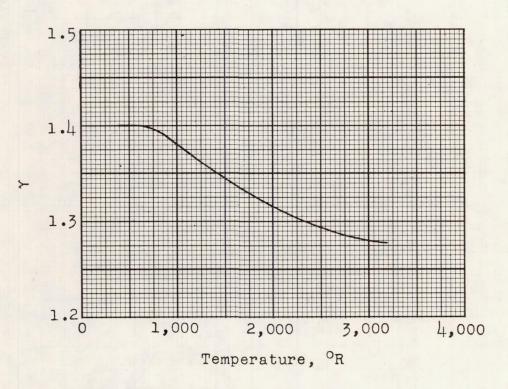
Figure 10.- Variation of adiabatic flame temperature with fuel-air ratio. Dissociation effects were neglected.
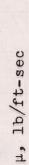
(a) Specific heat at constant pressure.
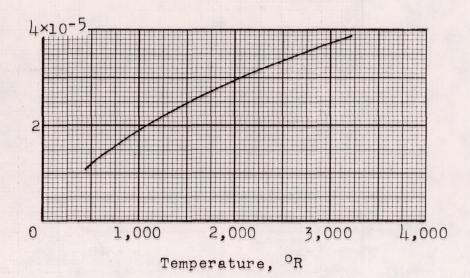
(b) Ratio of specific heats.
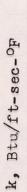
Figure 11.- Variation with temperature of the thermodynamic properties
of the exhaust gas.
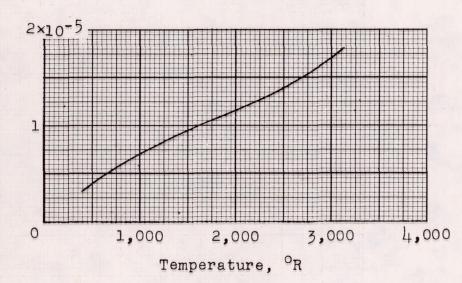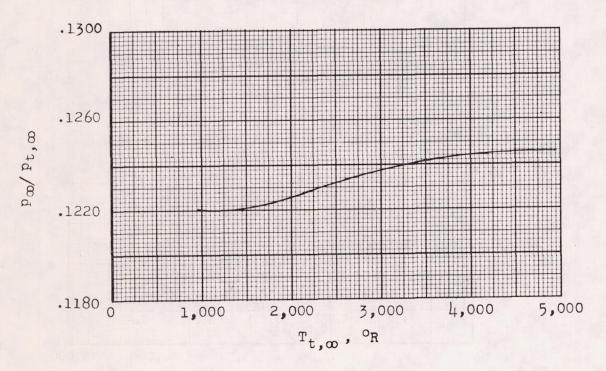
(c) Viscosity.

(d) Thermal conductivity.

Figure 11.- Concluded.
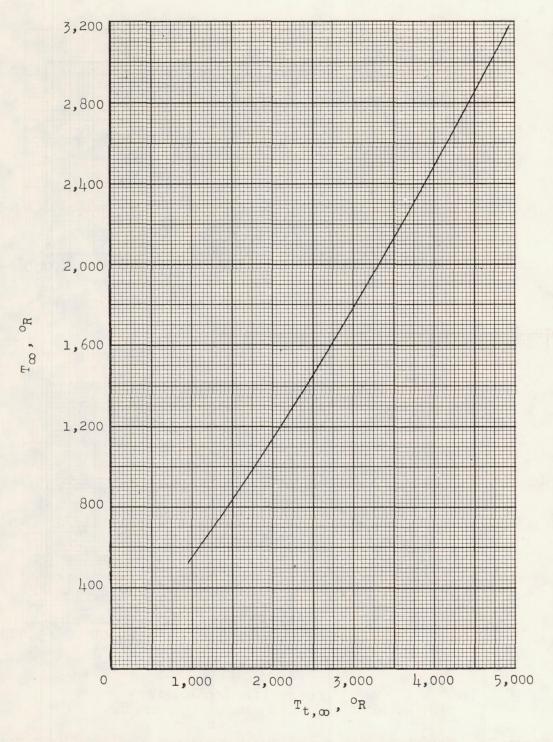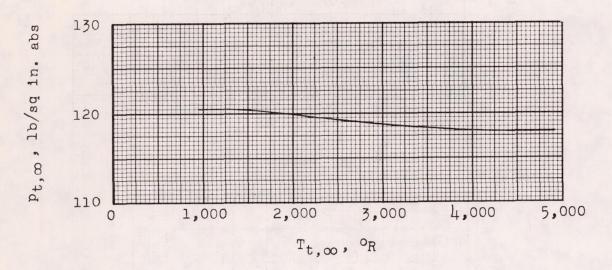
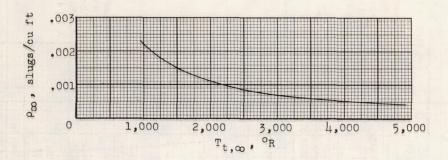Figure 12.- Variation of nozzle exit static temperature with stagnation temperature. M = 2.03.

(a) Stagnation pressure based on a static pressure of 14.7 pounds per square inch absolute.
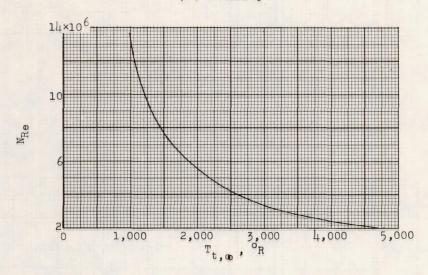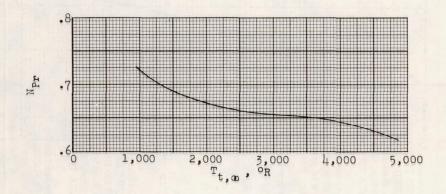

(b) Ratio of static to stagnation pressure.

Figure 13.- Variation with stagnation temperature of stagnation pressure and the ratio of static to stagnation pressure in the test section.

(a) Density.

(b) Reynolds number based on a length of 1 foot.

(c) Prandtl number.

Figure 14.- Variation of density, Reynolds number based on a length of
1 foot, and Prandtl number with stagnation temperature.